Wavelength selective modulation in femtosecond pump–probe spectroscopy and its application to heme proteins

Florin Rosca, Anand T. N. Kumar, Dan Ionascu, Theodore Sjodin, Andrey A. Demidov, and Paul M. Champion[a)]
Physics Department and Center for Interdisciplinary Research on Complex Systems, Northeastern University, Boston, Massachusetts 02115

(Received 13 December 2000; accepted 19 February 2001)

We demonstrate novel lock-in detection techniques, using wavelength selective modulation of ultrafast pump and probe laser pulses, to discriminate between vibrational coherence and electronic population decay signals. The technique is particularly useful in extracting low frequency oscillations from the monotonically decaying background, which often dominates the signal in resonant samples. The central idea behind the technique involves modulating the red and/or blue wings of the laser light spectrum at different frequencies, Ω_R and Ω_B, followed by a lock-in detection at the sum or difference frequency, $\Omega_R \pm \Omega_B$. The wavelength selective modulation and detection discriminates against contributions to the pump–probe signal that arise from degenerate electric field interventions (i.e., only field interactions involving different optical frequencies are detected). This technique can be applied to either the pump or the probe pulse to enhance the off-diagonal terms of the pump induced density matrix, or to select the coherent components of the two-frequency polarizability. We apply this technique to a variety of heme-protein samples to reveal the presence of very low-frequency modes ($\sim$20 cm^{-1}). Such low-frequency modes are not observed in standard pump–probe experiments due to the dominant signals from electronic population decay associated with resonant conditions. Studies of the diatomic dissociation reaction of myoglobin (MbNO$\rightarrow$Mb+NO), using wavelength selective modulation of the pump pulse, reveal the presence of an oscillatory signal corresponding to the 220 cm^{-1} Fe–His mode. This observation suggests that the spin selection rules involving the ferrous iron atom of the heme group may be relaxed in the NO complex. Mixed iron spin states associated with adiabatic coupling in the MbNO sample could explain the fast time scales and large amplitude that characterize the NO geminate recombination. © *2001 American Institute of Physics.* [DOI: 10.1063/1.1363673]

I. INTRODUCTION

Femtosecond coherence spectroscopy (FCS) is a pump–probe technique that utilizes the bandwidth of femtosecond laser pulses to prepare and monitor coherent states in a wide variety of samples.[1–10] This technique allows the real-time observation of ultrafast processes. Following pump pulse excitation of a resonant two electronic level system, two types of processes can occur that we refer to as ''field driven'' and ''reaction driven.'' In the first case the pump pulse excites the Raman active modes of the sample without affecting its structure. In the reaction driven case, the excited electronic state rapidly decays into other electronic states due to nonradiative surface crossing, and the system is left in a coherent ''product state.'' The delayed probe pulse monitors the change in the sample absorption induced by the pump pulse.

In this work we focus on the detection of time resolved low-frequency vibrational modes in heme proteins. The heme proteins form a large class of biomolecules, which are involved in a variety of important biochemical reactions such as diatomic ligand storage and transport, enzyme catalysis, and electron transport. The iron atom, placed at the center of the heme group (active site), can reversibly bind diatomic molecules like NO, CO, and O_2. Here, we study the ferric and ferrous unbound species as well as the NO bound state. We have developed wavelength selective modulation techniques to detect low-frequency vibrational modes coherently driven by a pump pulse resonant with the Soret absorption band of the heme chromophore. The low-frequency modes detected[11,12] in heme proteins are conceivably connected to the energy transport between the active site and the protein backbone,[13–15] which is expected to be important to the physiological functionality of the protein.

The signals generated using FCS under resonant conditions consist of damped oscillations corresponding to the vibrational modes excited by the pump pulse, along with a superimposed monotonically decaying background, usually related to processes like electronic relaxation, ligand recombination (for the samples involving photodissociation), and vibrational cooling. Vibrational oscillations below 400 cm^{-1} are accessible using pulses of $\sim$50 fs. The main goal of the present paper is to demonstrate experimental techniques that resolve the vibrational part of the signal from the monotonically decaying background. The motivation for this endeavor is the fact that very low-frequency modes ($<$40 cm^{-1}) are quite difficult to recover from the data by signal processing when they are superimposed on a strong (and often nonex-

a)Electronic mail: champ@neu.edu

ponential) monotonically decaying background.

Various data analysis methods are currently used to extract the oscillatory components from the data.[16] One popular method is a linear predictive singular value decomposition (LPSVD) algorithm[17,18] that uses decaying exponentials to fit the monotonically decaying part of the signal and, at the same time, fits the oscillatory part of the signal using damped cosine functions. An alternative way of fitting the experimental data is through a maximum entropy method (MEM) algorithm that fits the monotonic part of the signal using exponentials with a continuous distribution of decay rates. The oscillatory part of the signal that is left after using MEM to extract the background can be analyzed using LPSVD or a Fourier transform algorithm. The power spectra generated using both methods are usually in excellent agreement. However, as the oscillatory frequency is lowered, both methods of analysis begin to generate unsatisfactory results in the presence of a strong monotonic background. In this paper we offer an experimental solution to this problem.

One method of extracting the vibrational signal from the monotonic background arises from the fact that these two types of signal are generated differently. A major component of the monotonic background is the population decay of excited states, which does not require the spectral bandwidth available within the laser pulse to generate signal. If we consider a second order electric field interaction for each of the pump and probe pulses (which is the lowest order that can contribute to the four wave mixing signal), the two field interventions involved in the pump (or probe) interaction will have to involve identical frequency components from the laser bandwidth in order to create (or monitor) an electronic and/or vibrational population. On the other hand, a vibrational coherence needs the spectral bandwidth of both the pump and probe pulses in order to be observed. Two fields of different optical frequencies ($\omega_1-\omega_2=\omega_j$) are needed within the pump (or probe) spectral bandwidth in order to create (or detect) a coherence at frequency ω_j. We have used the different electric field dependence of the population and coherence terms to develop a technique that differentiates between these two sources of signal. This technique involves wavelength selective modulation of the spectral components of the pump and probe laser pulses. A detailed presentation of the technique and its ability to resolve the oscillatory part of the signal from the monotonic background is presented below.

II. MATERIALS AND METHODS

We use a self-mode-locked Ti:sapphire laser (Verdi Pumped Mira 900, Coherent Inc.) to generate the pump/probe laser pulses used in this work. The laser generates femtosecond pulses (45–100 fs) with a center wavelength between 700 and 960 nm. When trying to detect low-frequency modes we use the longest pulses available (80–100 fs). A 0.2 mm BBO crystal is used to double the IR light in order to obtain blue pulses, resonant with the Soret absorption band of the heme proteins under study (420–435 nm). In all experiments discussed here, the pump and probe light have the same spectral content. The average power of blue light at the sample is 30 mW, which corresponds to about 0.4 nJ per pulse pair. A pump–probe pulse pair affects less than 1% of the sample. We use a ~3.5 inch spinning cell, rotating at ~3500 rpm, to refresh the sample in the illuminated volume. Under these conditions, there is no build-up of unligated species in the NO bound samples.

Potassium phosphate buffer (pH=7.8, 0.1 M) is used to dissolve the protein, and 2 μl of 1 M dithionite solution is added to 90 μl of buffered sample to obtain the deoxy species. An additional 1 μl of 1 M $NaNO_2$ solution is added to prepare the NO adduct. The protoporphyrin IX (FePPIX) solution was prepared with the addition of 0.1 M 2-methylimidazole (which coordinates to Fe) and 1.5% cetyl trimethyl ammonium bromide (CTAB), to prevent sample aggregation. The microperoxidase-8 (MP8) solution was prepared with the addition of 1.5% detergent (CTAB), to prevent sample aggregation. The octaethylporphyrin (OEP) was diluted in an aqueous sodium dodecyl sulphate (SDS) detergent micellar solution,[19] with the addition of 2 M 2-methylimidazole (which coordinates to Fe). The H93G Mb sample was provided by Professor Doug Barrick (John Hopkins University, Department of Biophysics) and was prepared according to standard procedures.[20,21] The concentration of protein is chosen so that the sample has an absorbance of about 0.6 OD at the pump wavelength in a 0.5 mm cell.

The pump–probe setup[11] is shown in Fig. 1 and involves a grating pair to disperse the probe [Fig. 1(a)] or the pump [Fig. 1(b)] beams. The dispersed light is collimated by a lens and is reflected back by a mirror. The distances between these three optical elements (grating–lens, lens–mirror) are equal to the focal length of the lens. This is a regular pulse shaping geometry[22] in which the grating is used in a double-pass configuration. The returning beam makes a slight angle with the incident one, such that it can be picked off on the edge of another mirror after the second reflection off the gratings. The chirp is being compensated by a double prism setup for the undispersed beam and for the dispersed beam the position of the lens (L3) is varied.[23] An acousto-optic modulator (AOM) (Neos Tecnologies) is used to modulate the pump beam at 1.5 MHz. The pump–probe delay time is varied using a 1 μm step translation stage (SM).

In Fig. 1(a), we show how the probe beam is dispersed by the grating pair and modulated at selected wavelengths. The AOM is placed on the other beam, the pump, which is not dispersed. For the application presented here, a fork chopper (CH10 made by Boston Electronics) (FC) is placed on the dispersed beam in front of mirror M3 to modulate half of the probe's spectrum at 900 Hz. Due to the fact that the final signal is detected at the working frequency of the fork chopper, only the modulated part of the third-order polarization (generated by the modulated part of the third field's spectrum) will be detected in the final signal. Thus, the chopped part of the probe spectrum defines the spectral content of the third field involved in signal generation in this four wave mixing experiment. After the sample, the probe beam is again dispersed by a grating. The modulated part of the probe spectrum is blocked, so that only the unmodulated half of the probe spectrum is incident on the photodiode [see Fig. 1(a)]. The detected part of the probe spectrum defines

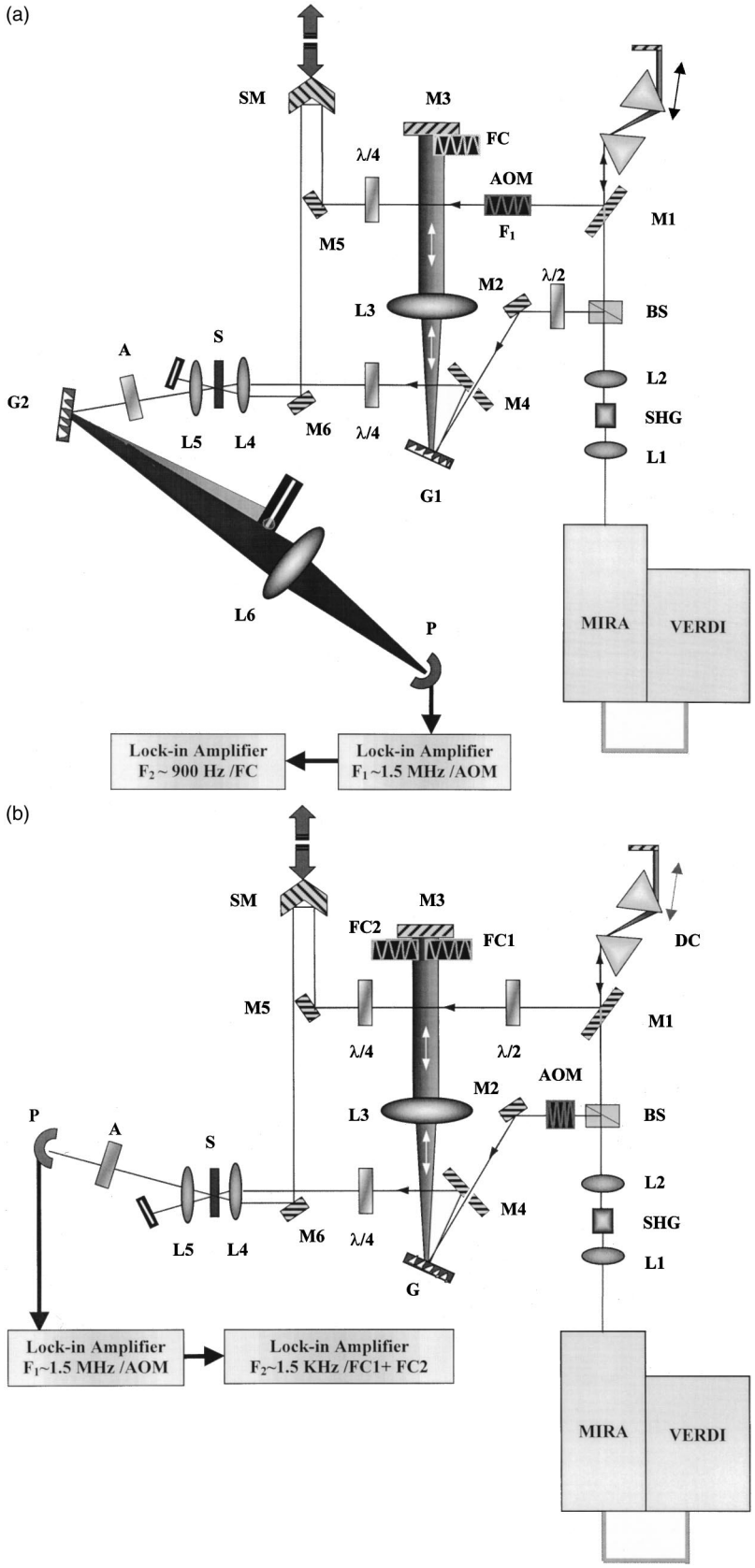

FIG. 1. (a) Description of the experimental setup used for the frequency selective probe modulation. The probe beam is dispersed using a first grating (G1), collimated by a lens (L3), and reflected back by the mirror M3. The fork chopper (FC) used to modulate parts of the probe spectrum is placed in front of M3. After the sample, the probe beam is dispersed again (using G2) and the unchopped part of it is detected with a photodiode (P). The signal is processed by two cascaded lock-in amplifiers. The symbols used in the figure are: lenses: L1–6, second harmonic generating crystal: SHG, beam splitter: BS, mirrors: M1–6, dispersion compensator: DC, acousto-optic modulator: AOM, half waveplate: λ/2, quarter waveplate: λ/4, diffraction gratings: G1 and G2, fork chopper: FC, stepping motor: SM, sample cell: S, polarization analyzer: A, photodiode: P. (b) Description of the experimental setup used for the frequency selective pump modulation. The pump beam is dispersed using a grating (G). Two fork choppers (FC1 and FC2) are used to modulate parts of the pump spectrum. The full spectral content of the probe beam is detected with a photodiode (P). The second lock-in amplifier is triggered by the sum of the two chopper frequencies (FC1+FC2).

the spectral content of the fourth field. Because of this, the detected signal will arise from the distinct spectral contents of the third-order polarization and the final electric field intervention.

The pump and probe beams are focused into a rotating sample cell using a 2 in. lens. The pump beam is spatially blocked and selected against by a polarization analyzer, provided that the pump and probe beams have perpendicular polarization. The output of the photodiode is fed into the first lock-in amplifier (SRS 844) phase locked to the acousto-

optic modulator. The time constant on this first lock-in is set at 100 μs so that the signal at 900 Hz will not be averaged out. The output of the first lock-in is fed into a second one (SRS 850) that is phase locked to the 900 Hz fork chopper. The time constant of this lock-in is set to 300 ms, which is comparable to the waiting time of 200 ms spent by the stepping motor (SM) at each delay point. The autocorrelation is run under the same conditions as the experiment in order to account for the delay in the time response of the lock-in and provide an accurate pump–probe zero delay. The second lock-in generates the final recorded signal. The motivation for this setup will be addressed in more detail below.

When we apply the wavelength selective modulation technique to the pump beam, the pump must be dispersed [Fig. 1(b)]. Two fork choppers working at different frequencies (Ω_R=900 Hz and Ω_B=600 Hz) are used to modulate the red and blue halves of the pump's spectrum (e.g., see also the top right panel of Fig. 8). The AOM is also placed on the pump beam. After the sample the pump beam is again blocked and the full spectrum of the probe is detected by a photodiode (P). The output of the photodiode is fed into the first lock-in amplifier, with the time constant set at 100 μs, phase locked to the AOM at 1.5 MHz. The output of the first lock-in is fed into the second one, which is phase locked to the sum of the two chopper frequencies (Ω_{SUM}=1.5 kHz). To generate the sum frequency we use a frequency mixer to mix the two initial frequencies and an electronic filter (model 3382, Krohn Hite Corp.) to select the sum from the initial frequencies and their difference. In order to generate signal that will be detected by the second lock-in (at $\Omega_R+\Omega_B$) the two pump field interventions have to be modulated at Ω_R and Ω_B, respectively. The two fork choppers are placed on the dispersed pump beam's spectrum such that the spectral components modulated at Ω_R and Ω_B do not overlap. The two pump field interventions will consequently have distinct spectral content.

III. WAVELENGTH SELECTIVE MODULATION OF THE PROBE PULSE

The self-mode-locked Ti:sapphire laser produces pulses (τ=50 fs) that can excite and probe vibrational coherences within its spectral bandwidth (~400 cm^{-1}). For biomolecules, the low-frequency modes (under 100 cm^{-1}) are of special importance because, if they are more delocalized, they may be involved in energy and information transport. For example, in heme proteins, the doming mode of the heme is expected[24,25] below 100 cm^{-1}.

We have previously discussed the methodology of detuned detection to selectively enhance the low- or high-frequency part of the measured signal.[11,12,26,27] In the detection scheme for detuned detection the probe beam is dispersed using a monochromator, and a photomultiplier tube detects a selected narrow bandwidth within the probe's spectrum. We have shown that detection close to the carrier wavelength of the probe pulse spectral distribution selectively enhances the low-frequency modes (and the ''zero frequency,'' monotonic background signal), while detection in the wings of the spectral distribution enhances only the high frequency modes.

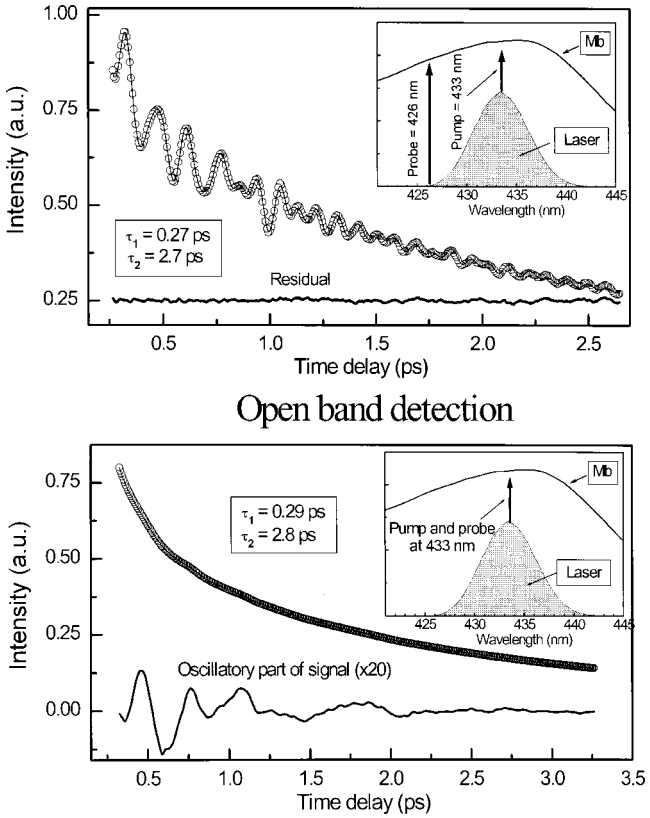

FIG. 2. FCS signal from deoxy Mb using detuned detection (upper panel) and open band detection (lower panel). The circles are experimental data points and the solid line is the LPSVD fit. The insets show the absorption spectrum of deoxy Mb, the spectrum of the laser pulse (grayed), and the detection conditions. Two exponential decay times characterize the monotonic background of the FCS signal.

For the more commonly employed ''open band'' detection, a photodiode is used to detect the full spectrum of the probe beam and, once again, both the low-frequency part of the sample's vibrational spectrum and the background signal are enhanced. In Fig. 2 we present examples of data generated using deoxy Mb with both detuned (upper panel) and open band detection (lower panel). As seen in the detuned measurements of Fig. 2, the high frequencies are selected over the decaying background, whereas in the open band measurements the low-frequency oscillations ride on a very strong background signal. This can be intuitively understood if we think of the monotonically decaying background as a zero frequency signal, which is enhanced along with the low-frequency modes. The lower the frequency of the mode we are trying to detect, the harder it will be in the data analysis to separate it from the background.

One of the novel aspects of the present work involves the experimental discrimination between the background and the low-frequency modes. In order to explain the technique, we first need to discuss the key differences between the origin of the background and the oscillatory signals.

After the pump pulse interaction, vibrational coherence is induced in the sample, as manifested in the off-diagonal terms of the second order density matrix. The delayed probe pulse monitors the subsequent nonequilibrium response of the medium, which includes vibrational and electronic popu-

lation decay in addition to vibrational coherences. The pump–probe signals are readily analyzed in the well-separated pulse limit, where the pump and probe pulses are temporally separated.[28] The generation of the third-order polarization and its subsequent detection have been studied using density matrix pathways[26,27] and the doorway window picture.[29,30] For the present analysis, it is convenient to express the polarization in terms of the two frequency polarizability,[31,32] $\alpha(\omega,\omega')$, which reflects the nonstationary response of the medium induced by the pump pulse. If we denote the spectral envelope of the probe pulse electric field as $E_b(\omega)$, the third-order polarization can be expressed as

$$P(\omega,\tau)=\int_{-\infty}^{\infty} d\omega'\ \alpha(\omega,\omega')E_b(\omega')e^{i\omega'\tau}, \tag{1}$$

where τ is the pump–probe delay time. The final open band detected signal is obtained as the overlap of the final probe field with the third-order polarization

$$S(\tau)=\int_0^{\infty} d\omega\ \omega\ \mathrm{Im}[E_b^*(\omega,\tau)P(\omega,\tau)e^{-i\omega\tau}]. \tag{2}$$

The two-frequency polarizability $\alpha(\omega,\omega')$ has the following typical form:

$$\alpha(\omega,\omega')=\alpha_0(\omega)\,\delta(\omega-\omega')+\sum_j\ \alpha_j(\omega)\,\delta(\omega-\omega'\pm\omega_j), \tag{3}$$

where the summation is over all the vibrational frequencies ω_j present in the system. $\alpha_0(\omega)$and $\alpha_j(\omega)$ are functions that depend on the electron–nuclear coupling and the pump induced displacement for the mode ω_j as well as other properties that govern the line shape of the system. It is clear from the above expressions that the oscillatory parts of the pump–probe signal arise from the off-diagonal parts (i.e., $\omega\neq\omega'$) of $\alpha(\omega,\omega')$. These oscillatory signals are hence observed only when the frequency components of the second probe field in Eq. (2) are different from those of the first field in Eq. (1) that generated the third-order polarization. More precisely, the two optical frequencies involved in signal generation must be separated by the vibrational mode frequency ω_j. It is clear from Eq. (1) that the resulting third-order polarization consists of blue- and redshifted spectral functions, proportional to $E_b(\omega\pm\omega_j)$, which correspond to coherent anti-Stokes and Stokes Raman spectroscopy (CARS and CSRS resonances)[26,27,33] [here, we assume that $\alpha_j(\omega)$ is slowly varying with respect to $E(\omega)$]. In contrast, the monotonically decaying (zero frequency) background signal is proportional to the ''diagonal'' parts of $\alpha(\omega,\omega')$, which are observed only when the third and fourth field interactions have the same optical frequency (i.e., $\omega=\omega'$).

Now, consider the case where a wavelength selective modulation is applied to one half of the probe pulse spectrum on either the red or the blue side of the center (carrier) wavelength. The third order polarization detected by the lock-in is generated by the modulated half of the spectrum, so that the final signal in Eq. (2) can be obtained by monitoring the other half of the probe spectrum, as shown in Fig. 1(a). In Fig. 3, we show the case where the red half of the probe

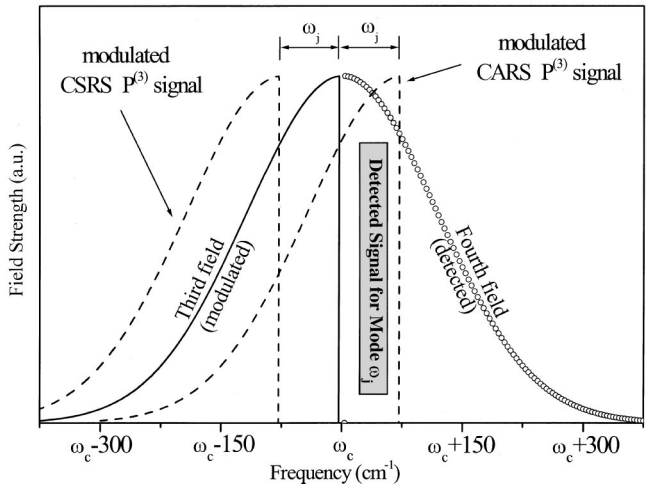

FIG. 3. Graphic scheme depicting the spectral structure of the probe field interventions that generate the observed signal. The solid line is the modulated half of the probe spectrum (third field). The dashed line represents the detected third-order polarization, shifted from the carrier frequency by the energy of the observed vibrational mode. The circles represent the detected half of probe pulse spectrum (fourth field). The measured signal is generated in the overlapping spectral region between the modulated part of the third-order polarization and the fourth field.

pulse spectrum is modulated and the Stokes and anti-Stokes shifted components of the modulated part of the polarization are also shown. Since we selectively detect only the unmodulated part of the probe pulse spectrum, the overlap of the CARS (anti-Stokes) shifted polarization and the unmodulated half of the probe pulse spectrum determines the final signal as described by Eq. (2). It is clear that the overlap is nonzero only if $\omega_j\neq 0$. In other words, the background ($\omega_j=0$) components of the pump–probe signal can be experimentally eliminated using this approach. In order to completely eliminate the background signal, no modulated probe light can be allowed to reach the photodiode. However, due to the finite resolution in selecting the detected portion of the light, it is sometimes necessary to let some of the modulated probe light reach the detector. In this way we can be certain that the fields necessary for the detection of very low-frequency modes (spectrally very close to the modulated light) are present. As a result, the low-frequency modes will sometimes ride on a small background signal.

One possible concern related to this technique is that the temporal shape of a pulse with a non-Gaussian spectral distribution might affect the measured signal. To study this possibility, we performed a series of control experiments in order to define the conditions under which the ensuing signal contains the expected oscillatory components without any distortions or artifacts. In Fig. 4 we present the signals obtained using deoxy myoglobin (Mb^{2+}) under four different conditions. As described earlier, half the spectral content of the probe beam is chopped with a fork chopper. In the first panel we present the signal obtained if a 0.2 nm spectral window of the unchopped portion of the probe light is detected. This window is placed 165 cm^{-1} from the cut made by the fork chopper in the probe spectrum. The signal that dominates under these conditions is a damped 165 cm^{-1} oscillation, symmetric around the zero delay time. Moving

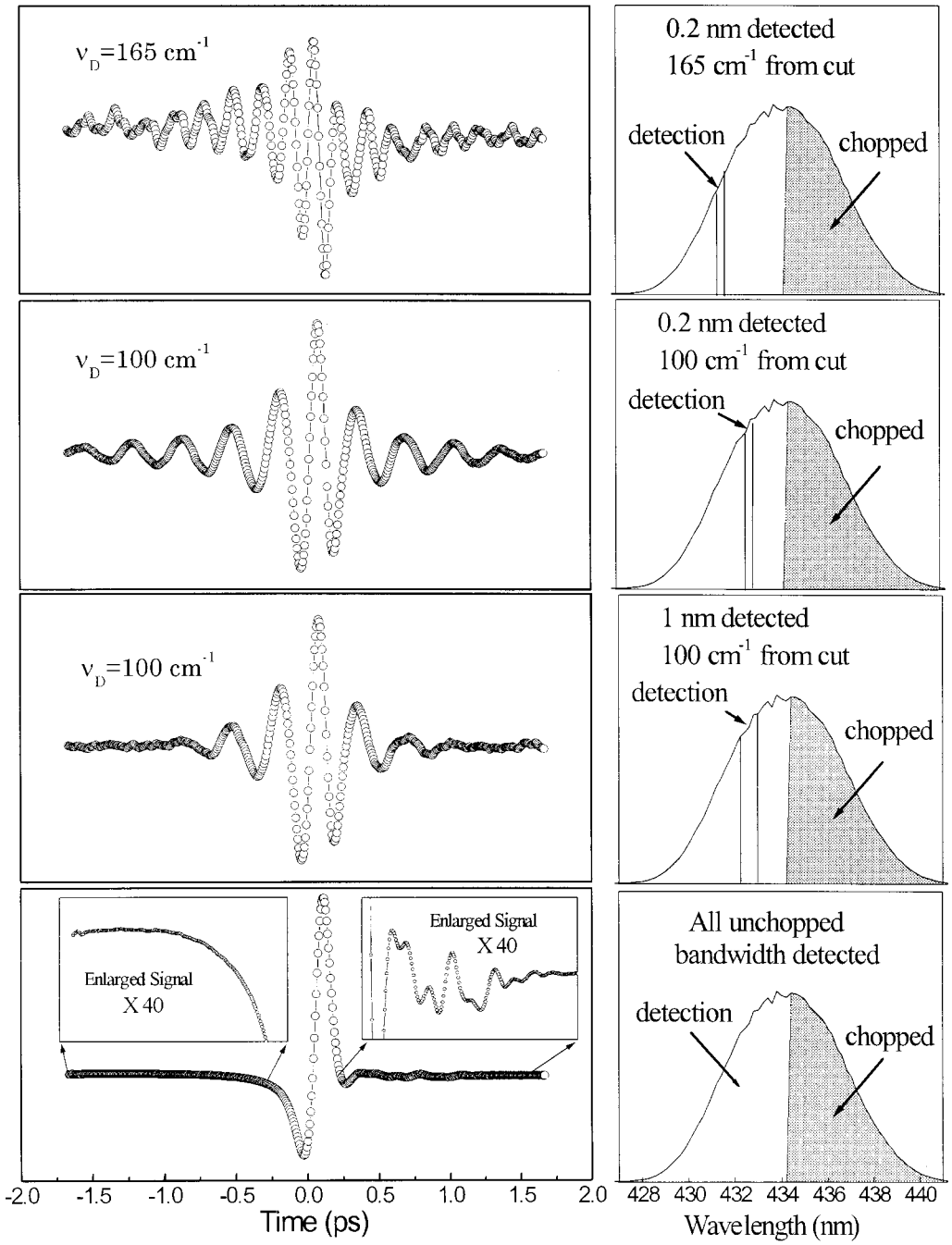

FIG. 4. Sequence of frequency selective probe modulation experiments on deoxy Mb under different detection conditions. Left panels present the generated FCS signals, whereas the right panels depict the detection conditions of the experiment. The grayed area is chopped by the fork chopper. In these experiments we used 55 fs pump/probe pulses with a 434 nm carrier wavelength.

the detection window to a new position, 100 cm^{-1} from the cut made by the fork chopper, changes the frequency of the observed oscillation to 100 cm^{-1}, as seen in the second panel. Increasing the width of the detected spectral window to 1 nm damps the observed oscillation, as seen in the third panel. The frequency of the damped symmetric oscillation is determined by the detuning between the edge of the fork chopper and the detection window, while the damping is determined by the width of the detection window. As seen in the fourth panel, the symmetric detuning oscillation can be completely damped if the entire unmodulated half of the probe spectrum is detected. The signal at negative time delays now shows just a monotonic decay, whereas at positive time delays we observe the oscillatory signal characteristic of deoxy myoglobin. Thus, by chopping half of the probe spectrum and detecting the entire bandwidth of the unchopped spectral regions one can detect the coherent oscillations of the material and experimentally discriminate against the monotonically decaying background. For all the data presented in this paper we have run symmetric scans and verified that no oscillatory signals were detected for negative time delays. This is the best method to ensure that the detected signals are a measure of the sample response, undistorted by the detection technique. Since a traditional autocor-

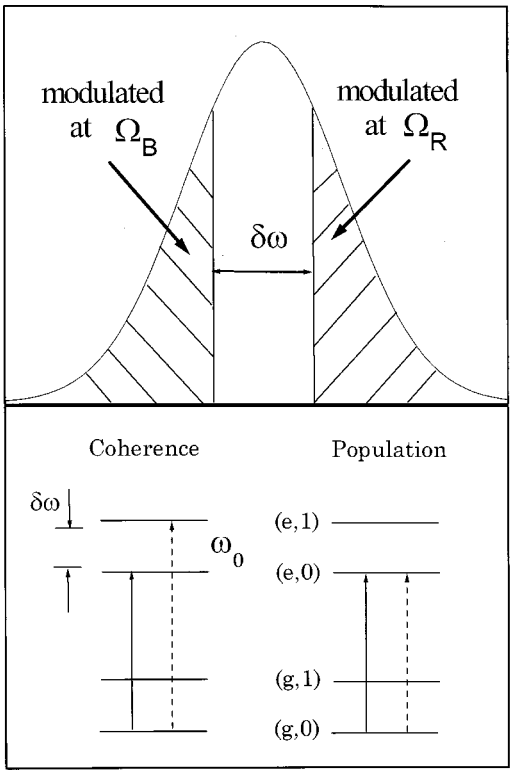

FIG. 5. (Upper panel) Description of the spectral modulation used on the pump beam. The red and blue parts of the spectrum are modulated at frequencies Ω_R and Ω_B. $\delta\omega$ is the width of the unmodulated spectral region between the two choppers. (Lower panel) Energy level diagrams describing the creation of a vibrational coherence in the excited electronic state and the population of the first vibrational level of the excited electronic state. The electronic states are labeled e (excited) and g (ground), the vibrational states are 0 and 1. The unmodulated gap width ($\delta\omega$) is compared to the energy of the excited state vibrational mode (ω_0). A similar picture can be easily constructed for ground state coherences.

relation measurement sums photons containing fields of the same wavelength, it yields no signal under these detection conditions.

IV. WAVELENGTH SELECTIVE MODULATION OF THE PUMP PULSE

In a density matrix description of the signal the diagonal elements represent the population terms, whereas the off-diagonal elements represent the coherence. In the previous section, we discussed how the different frequency components of the probe pulse can be modulated and detected to discriminate against the population decay contribution to the signal. In the present section, we discuss how a similar chopping scheme applied to the pump pulse can be used to select coherent oscillations based upon the optical frequencies of the fields needed for their generation. In this way, the signals arising from two pump fields of identical frequencies (expressed in the diagonal terms of the density matrix) can be suppressed.

As discussed earlier, two fork choppers are used to modulate the red and blue sides of the pump pulse spectrum at two different frequencies, Ω_R and Ω_B. This is schematically depicted in the top panel of Fig. 5, where the shaded regions correspond to the modulated blue and red sides of the pump pulse spectrum. The transmitted probe light is incident on a photodiode and, as described earlier, detected by the two cascaded lock-in amplifiers phase locked to the AOM (1.5 MHz) and to the sum frequency of the two fork choppers [see Fig. 1(b)]. In order to understand the mechanism behind the pump pulse modulation experiments, we take a density matrix approach. When interacting with a two electronic level system, a femtosecond pump pulse can induce vibrational coherence in both the ground and the excited electronic states. The nonstationary state induced by the pump pulse can be described using the second-order perturbative expression for the doorway density matrix for the ground and excited electronic states.[34,35]

In the Appendix, we consider a two-level system with a single linearly coupled mode (frequency ω_0), and present a simple analysis of the pump pulse modulation experiment for the excited state doorway density matrix ρ_e [Eq. (A1)]. Since only the signal modulated at the sum frequency $(\Omega_R+\Omega_B)$ is detected, only those terms of the second order density matrix with one field component from the red and blue wings of the pump pulse spectrum [$E_R(t)$ and $E_B(t)$ in Eqs. (A3a) and (A3b)] are relevant. It is shown in the Appendix that the elements of the density matrix $(\rho_e)_{vv'}$ induced by the field combinations $E_R E_B$ and $E_B E_R$ will be suppressed in the signal detected at $(\Omega_R+\Omega_B)$ if the condition $|(v-v')|\omega_0 < \delta\omega$ is satisfied [see Fig. 5 and Eq. (A5)]. Here, $\delta\omega$ is the frequency gap determined by the distance between the blades of the fork choppers that modulate the red and blue spectral parts of the pump pulse. In particular, the zero-frequency (background) signal, which corresponds to population decay, will be suppressed as long as $\delta\omega>0$. This suggests how we can use the capability of pump-wavelength modulation to selectively eliminate the contributions of the background from the measured probe response. In the Appendix, we also discuss how electronic and vibrational dephasing processes can affect the resolution of the wavelength selective modulation. While electronic dephasing does not affect the sharpness of the frequency selection, vibrational dephasing can affect the resolution of the wavelength selective modulation. Thus, the condition $\omega_0 < \delta\omega$ for suppression of the ω_0 fundamental will not be sharp, but will exhibit a smooth behavior as $\delta\omega$ is varied across the finite bandwidth of the vibrational mode.

If the blue and red modulated spectral regions (shaded in the upper panel of Fig. 5) are separated by an unmodulated region of width $\delta\omega$ (determined by the distance between the blades of the two fork choppers), the two fields that generate signal at $\Omega_R+\Omega_B$ will be energetically separated by at least $\delta\omega$. Two energy level diagrams are presented in the lower panel of Fig. 5, associated with two possible pump induced processes: the creation of excited state coherence and population. In this figure, we compare the energy of a vibrational mode (ω_0) to the spectral gap between the modulated regions ($\delta\omega$). For $\delta\omega=0$, when the fork choppers' vanes leave no unmodulated spectral region between them, any vibrational mode accessible within the pump pulse bandwidth will be detected, since the necessary field frequencies are available from each modulated spectral region (Ω_R and Ω_B). As soon as the choppers are separated to leave an unmodu-

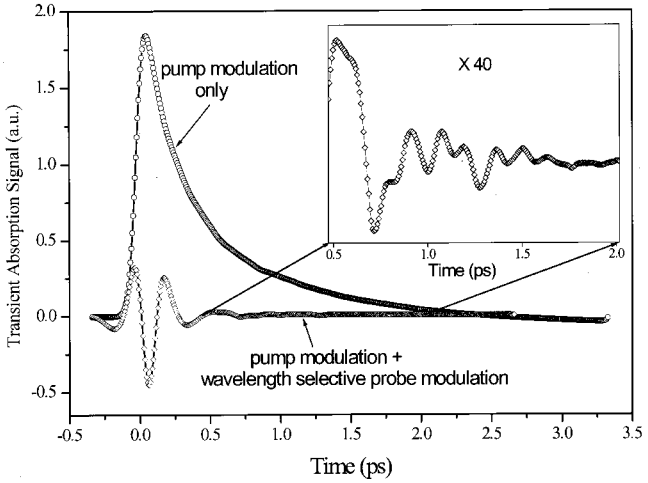

FIG. 6. Comparison between two experiments on deoxy Mb, one using a regular pump–probe setup with open band detection and the other using the frequency selective probe modulation technique. The background signal is almost completely removed and the oscillatory part of the signal (enlarged 40 times in the inset) is clearly exposed when using the second technique. We used 75 fs pump/probe pulses with a 442 nm center wavelength. In the frequency selective probe modulation experiment the red part of the probe beam is chopped and the blue part is detected with a photodiode.

lated region between them ($\delta\omega$), the availability of modulated fields is restricted. One can see that if the unmodulated gap is less than the frequency of the vibrational mode ($\delta\omega < \omega_0$), electric fields modulated at Ω_R and Ω_B are still available to generate the coherence associated with that mode. However, if the unmodulated gap becomes larger than the mode frequency ($\delta\omega > \omega_0$), the modulated fields can no longer generate a coherence at this frequency. Processes involving pump induced population dynamics (needing two fields of the same color) will not be detected by this method as long as the two choppers modulate distinct spectral regions and the detection is at the sum frequency $\Omega_R + \Omega_B$.

Potentially, this approach can distinguish the coherent response of an overdamped low-frequency mode from the population dynamics of electronic relaxation and cooling. It can also select against signals generated through processes like sequential dissociation of a ligand, which may involve the initial preparation of populations and the subsequent dynamics.[9,36]

V. APPLICATIONS TO HEME PROTEINS

A. Probe beam modulation

We have applied wavelength selective modulation techniques to heme protein samples in an attempt to more clearly reveal low-frequency modes in the absence of background. In Fig. 6 we compare traditional open band measurements of deoxy Mb to the signals generated using wavelength selective modulation of the probe pulse [Fig. 1(a)]. As predicted, the signal generated using the selective modulation of the probe pulse contains the oscillations in the absence of background. On the other hand, the traditional open band signal contains a strong, monotonically decaying background superimposed with the oscillations. The absence of the monotonic background signal in the data generated by wavelength selective modulation of the probe beam facilitates the detection of low-frequency oscillatory signals with significantly improved signal to noise.

An alternative way to enhance the detection of low-frequency modes vs background can in principle be achieved by employing a detuned detection scheme[11,12] (see Fig. 2). To optimize this scheme requires the availability of laser pulses with bandwidth on the order of the mode frequency (ω_0) as well as high monochromator resolution ($\ll \omega_0$). However, under these conditions only a relatively narrow portion of the low-frequency vibrational spectrum can be enhanced. In contrast, the selective probe modulation technique allows background free detection of a much broader portion of the low frequency spectrum. Moreover, the detuned detection scheme uses only a small fraction of the probe laser light. Thus, as the resolution is increased for better enhancement of the oscillatory signal vs background, a significantly smaller amount of light is available for detection. As a result, the signal to noise in the detuned detection scheme is reduced as the signal to background ratio is increased. In contrast, the wavelength selective modulation technique detects half of the probe spectral content, which leads to an improvement in signal to background without a decrease in the signal to noise ratio. In a detuned measurement, it is straightforward to find the dependence of the signal-to-noise ratio (S_N) as a function of the oscillatory signal to background ratio (S_B). Assuming statistical noise, this dependence is given by the following expression:

$$S_N \sim \exp\left(\frac{3\Omega_0^2 \ln 2}{4} - \frac{\ln^2 S_B}{8\Omega_0^2 \ln 2}\right) \tag{4}$$

where $\Omega_0 = \omega_0/\sigma$ and σ is the full width at half maximum (FWHM) of the spectral content of the pulse intensity $[E^2(\omega)]$, and ω_0 is the energy of the specific mode to be detected. This expression describes explicitly how the signal to noise decreases as the oscillatory signal to background ratio is enhanced by detuning the detection window away from the carrier wavelength (ω_c). Plots of Eq. (4) are given in Fig. 7 and demonstrate how this decrease becomes more acute for lower frequency modes ($\omega_0 < \sigma$, $\Omega_0 < 1$). As expected, when the mode frequency begins to exceed the bandwidth of the laser pulse ($\omega_0 > \sigma$, $\Omega_0 > 1$), the signal also diminishes.

Since wavelength selective modulation does not suffer a decrease in signal to noise as the signal to background is increased, it is the preferred method for the detection of low-frequency modes. For example, when the time delay scan range is increased and the pulses are broadened to ~100 fs, wavelength selective modulation of the probe pulse allows us to observe a mode near 20 cm^{-1} in heme proteins that cannot be clearly detected using traditional measurements. Open band measurements enhance low-frequency modes along with the monotonic background, such that the low-frequency oscillations cannot be reliably extracted by data analysis from the strong background. The background free oscillatory signal generated using the wavelength selective modulation of the probe beam enables reliable detection of low-frequency modes in FCS. In Figs. 8(A) and 8(B) we

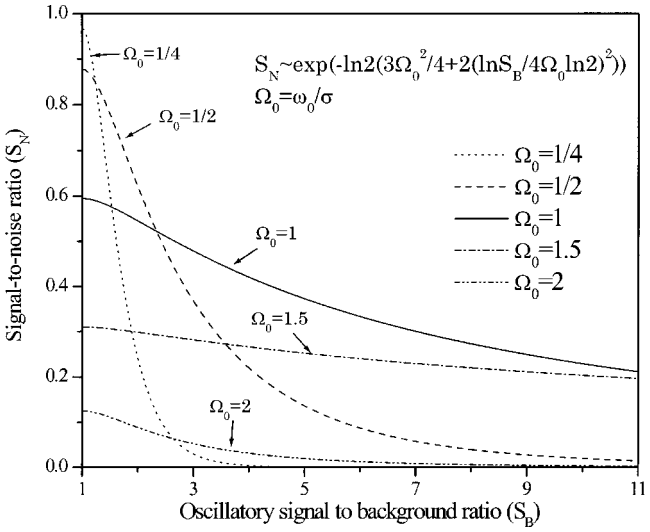

FIG. 7. Dependence of the signal-to-noise ratio (S_N) for the detuned detection scheme, as a function of the oscillatory signal to background ratio (S_B) for five values of Ω_0. Here, $\Omega_0=\omega_0/\sigma$ /σ, σ is the bandwidth of the laser light, and ω_0 is the energy of the specific mode to be detected. The plotted expression [Eq. (4)] describes explicitly how the signal to noise decreases as the oscillatory signal-to-background ratio is enhanced by detuning the detection window away from the carrier wavelength (ω_c). The expressions for S_N and S_B used to derive Eq. (4) are: $S_N \sim (E \cdot P^{(3)}(\Omega_0))^{0.5} \sim \exp(-x^2 \ln 2) \cdot \exp(-(x-\Omega_0)^2 \ln 2)$ and $S_B \sim P^{(3)}(\Omega_0)/E \sim \exp(-2 \ln 2(\Omega_0^2 - 2\Omega_0 x))$, where $x=(\omega-\omega_c)/\sigma$ is the detuning from the carrier wavelength normalized to the bandwidth of the laser, E is the intensity of the electric field, and $P^{(3)}(\Omega_0)$ is the third-order polarization for the mode ω_0. The units are arbitrary since frequency independent scaling factors have not been included.

present the oscillatory part of the signals obtained by applying this technique to a variety of heme protein samples. The background signal is decreased by at least an order of magnitude. The small amount of background present in the raw data, due to the finite resolution in selecting the detected portion of the light, has been removed using the LPSVD algorithm. The most notable feature[37] of the signal generated from ferrous myoglobin and ferrous protoporphyrin IX is the presence of a long lived mode near 20 cm^{-1}.

Results obtained on other samples containing Fe protoporphyrin IX as the active site demonstrate that the 20 cm^{-1} mode is sample dependent. A long-lived 23 cm^{-1} mode (see Table I) was observed in ferrous H93G myoglobin, a myoglobin mutant for which histidine 93 is replaced by a glycine (which does not coordinate to the heme iron) and 2-methylimidazole is ligated to the heme. In ferrous hemoglobin, the mode is detected at 26 cm^{-1} [see Fig. 8(A) and Table I].

We have also studied several heme proteins that do not contain protoporphyrin IX in the active site. For example, ferrous cytochrome c, ferrous microperoxidase and ferrous octaethylporphyrin do not show a low-frequency mode near 20 cm^{-1} [see Fig. 8(B) and Table I]. These results suggest[38] that the $\sim$20 cm^{-1} mode is protoporphyrin IX specific. In the NO bound species of ferrous myoglobin and hemoglobin, the 20–27 cm^{-1} mode is observed with a much shorter lifetime than in the unligated samples [see Fig. 8(A)]. This difference in lifetime is significant, because for the ligated samples the pump pulse triggers a photodissociation reaction. However, in both ligated and unligated samples, the probe pulse interrogates the unligated species.

Special precautions were taken to check for the reliability of the data showing the $\sim$20 cm^{-1} oscillations. Samples displaying a $\sim$20 cm^{-1} oscillation, as well as samples that do not display it, were run ''back to back'' (the sample cells were switched and run under identical experimental conditions) to ensure that the observed oscillatory signal is sample dependent. Long symmetric scans were measured, and the negative time delay (probe before the pump) signal was analyzed to check for the presence of symmetric damped oscillations, similar to those presented in Fig. 4. No such signals were found. Moreover, the 26–27 cm^{-1} mode in NO bound hemoglobin was detected using both the wavelength selective probe modulation technique and the standard open band detection experiment. The monotonic part of the open band generated signal for HbNO is first fit using the MEM algorithm and the residual oscillatory signal is fit using the LPSVD algorithm, which distinctly reveals the 26–27 cm^{-1} component in the power spectrum [dashed line in Fig. 8(A)]. This demonstrates definitively that the modes in the 20–27 cm^{-1} region are properties of the studied samples and independent of the detection technique.

B. Pump beam modulation

In the case of wavelength selective probe beam modulation, only processes that need probe fields of different colors to be detected are present in the final signal. The results of wavelength selective pump beam modulation are very similar to those obtained from probe beam modulation. When photostable samples are measured, the signal arising from population terms (i.e., the absorption of a photon with two identical pump field frequencies) generates a monotonically decaying background that is not passed through the second lock-in amplifier. In contrast, the vibrational coherences need two different color pump fields to be generated and they are modulated at Ω_R and Ω_B so that the coherence signal passes through the lock-in tuned to $\Omega_R+\Omega_B$.

It has previously been suggested[39] that samples undergoing a (nonadiabatic) photolysis reaction can lead to product state vibrational coherences that are triggered by the electron–nuclear coupling forces that develop during the photochemical reaction. In contrast to field driven coherences (which are created by pump fields of different color), the reaction driven coherences can, in principle, arise from pump induced electronic populations, which evolve rapidly to the final electronic product state. Upon the absorption of the pump photon, the system is projected onto an excited state potential and evolves, as the ligand dissociation takes place, towards the product state.[9] Such reaction driven coherences, if they are generated by pump fields of the same color, are not expected to appear in the pump beam modulation experiments. This is because the signals observed in the wavelength selective pump beam modulation experiments must be generated from a pump field intervention from each of the two different spectral regions modulated at Ω_R and Ω_B by the fork choppers. Only this ''off-diagonal'' component of the pump induced signal will be modulated at the

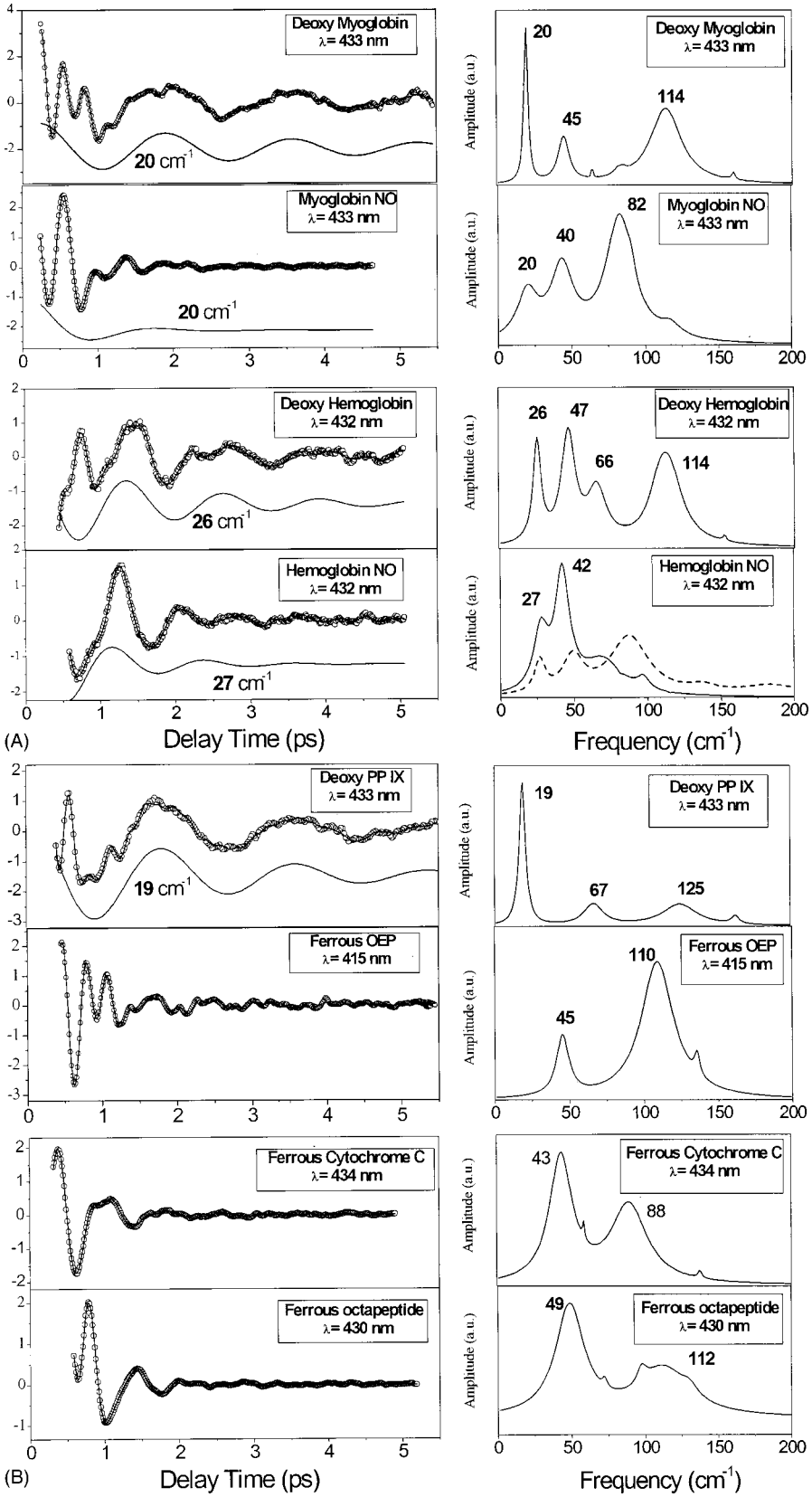

FIG. 8. (A) Sequence of experiments using frequency selective probe modulation on Mb and Hb. The left panels present the oscillatory part of the generated signal and the right panels show the corresponding power spectra. The 20–27 cm^{-1} oscillation extracted from the LPSVD fit is shown displaced from the data for the samples that display this mode. A second power spectrum (dashed line) for HbNO corresponds to the signal measured using open band detection. The vibrational mode near 27 cm^{-1} is a common feature observed using both detection conditions. (The mode at 42 cm^{-1} in the lower right panel is anomalously low in this data set and is normally found near 47 cm^{-1}.) (B) A similar sequence of experiments on heme model compounds and cytochrome c.

sum of the fork chopper frequencies $(\Omega_R+\Omega_B)$ and be detected by the second lock-in amplifier.

The oscillatory signals obtained by applying the wavelength selective pump beam modulation technique to NO bound myoglobin are presented in Fig. 9. The small residual monotonic background (that has been subtracted from the presented data) is probably related to the vibrational damping which affects the resolution of the technique (see the discussion in the Appendix). For the data presented in the first panel, the vanes of the two choppers were placed as

TABLE I. The frequency and lifetime for the 20 cm^{-1} mode in heme systems. The frequency (v in cm^{-1}), period of oscillation (T in ps), lifetime γ^{-1} in ps) and line width (y in cm^{-1}) of the ~20 cm^{-1} mode are displayed for the studied heme proteins. The estimated uncertainty for the frequency is ~2 cm^{-1}. The associated lifetime uncertainty is about 25%.

Sample	v (cm^{-1})	T (ps)	γ (cm^{-1})	γ^{-1} (ps)
Myoglobin				
Deoxy myoglobin	20	1.66	4.2	2.5
NO bound myoglobin	20	1.66	13.2	0.8
Deoxy H93G myoglobin	23	1.45	5.9	1.8
Met myoglobin	···			
Hemoglobin				
Deoxy hemoglobin	26	1.28	6.6	1.6
NO bound hemoglobin	26	1.28	13.5	0.8
Model compounds				
Ferrous FePPIX+2Me−Im	20	1.66	5.3	2
Ferrous OEP+2ME–Im	···			
Cytochromes				
Ferrous cytochrome C	···			
Ferrous octapeptide	···			

close to one another as possible, without being overlapped (see the inset in the top right panel of Fig. 9). If there was overlap, the spectral region modulated by both choppers would contain optical frequencies modulated at $\Omega_R+\Omega_B$, leading to the detection of background signal, as in the standard experiments. If a small gap is left between the chopper vanes to optimally suppress the detection of background signal, this will also select against the detection of the ~20 cm^{-1} mode. Under typical pump beam modulation conditions, the full vibrational spectrum (above ~20 cm^{-1}) allowed by our temporal resolution is observed. The observation of oscillatory signals when using wavelength selective pump beam modulation implies that two field interventions having different colors trigger the detected vibrational coherences. The need for different optical frequencies in generating the vibrational coherences in MbNO is further exemplified in the lower panels of Fig. 9. If the vanes of the two fork choppers are moved to leave between them a spectral region ($\delta\omega$) that is not modulated (see the insets in the lower right panels of Fig. 9), vibrational modes of frequency less than $\delta\omega$ can no longer be detected at $\Omega_R+\Omega_B$. This is due to the fact that the two pump field frequencies, each from a spectral region modulated by one of the fork choppers, cannot be closer to one another than the width of the unmodulated spectral region. It can be seen that, as the two vanes are moved further apart, more and more low frequency modes disappear from the FCS signal (see the power spectra). The wavelength selective pump beam modulation technique can therefore also be a useful tool to filter and isolate the modes of interest. It is especially noteworthy that the Fe–His mode, which is Raman inactive in MbNO, also disappears as the unmodulated gap between the fork choppers exceeds 220 cm^{-1}.

VI. DISCUSSION

We have developed novel wavelength selective modulation techniques that can be used to distinguish between the coherence and population terms in the signals generated by pump–probe femtosecond spectroscopy. Within a density matrix description, these techniques are sensitive to the off-diagonal terms (coherences), and discriminate against the diagonal terms (populations), which contribute to the signal. One motivation for developing these techniques is to obtain coherent signals, free from the population induced background decay that is often present in resonant samples. The work described here presents an experimental solution to the problem of separating the oscillatory part of the signal from the monotonically decaying background, a task that was previously addressed in the data analysis.

Using these new experimental methods we are able to observe modes having frequencies as low as 20 cm^{-1} in some heme proteins. We also observed this mode in a protoporphyrin IX model compound, where a detergent micelle, rather than the protein backbone, surrounds the heme. The porphyrin macrocycle is a ringed structure containing 20 carbon atoms bound to an inner core of 4 nitrogens. Off the outer macrocycle, there are eight sites where substituent groups can be bound (R_1-R_8). Iron protoporphyrin IX (FePPIX) is an asymmetric porphyrin with two vinyl groups bound at R_2 and R_4, and two propionic acid groups at R_6 and R_7. Horse heart myoglobin contains a FePPIX active site, which is covalently bound to the protein solely by a histidine (His93) coordinated to the iron. The presence of the 20 cm^{-1} mode in the FePPIX model compound, which has no amino acid backbone surrounding it, indicates that the observed mode is localized at the heme. The mode near 20 cm^{-1} appears only in samples containing iron protoporphyrin IX and its frequency is sample dependent. It is noteworthy that most normal mode calculations[24,25] do not predict modes of such a low-frequency to be localized at the heme. This is because these calculations are made considering only a bare porphyrin macrocycle (porphine), without the substituent groups present in FePPIX. Since the normal mode calculations[24] predict the doming mode to be around 50 cm^{-1} (the doming motion involves primarily the porphyrin core), it is conceivable that the addition of the substituent groups could induce the presence of even lower frequency modes in FePPIX. For example, calculations by Findsen *et al.*[40] suggest that coherences between 20–35 cm^{-1} can be assigned to torsions of the heme vinyl groups. Thus, one possible (but speculative) explanation of the strongly coupled, heme localized, mode near 20 cm^{-1} is that it corresponds to vinyl isomerization following excitation in the Soret band. Such isomerization can be viewed as analogous to the behavior of conjugated polyenes and would help to explain the absence of the ~20 cm^{-1} modes in samples that lack the vinyl groups (see Table I).

A broad peak near 25 cm^{-1}, associated with the collective oscillations of the polypeptide chain, has also been observed in recent high-resolution synchrotron based experiments[41] that are sensitive only to the vibrational spectrum of the ^{57}Fe at the active site of Mb. Similar features (~20 cm^{-1}) were observed in inelastic neutron scattering from hydrated protein films[42,43] and in site-selected fluorescence spectra of Zn-substituted Mb.[44] These experiments, along with protein density of state calculations,[45] indicate

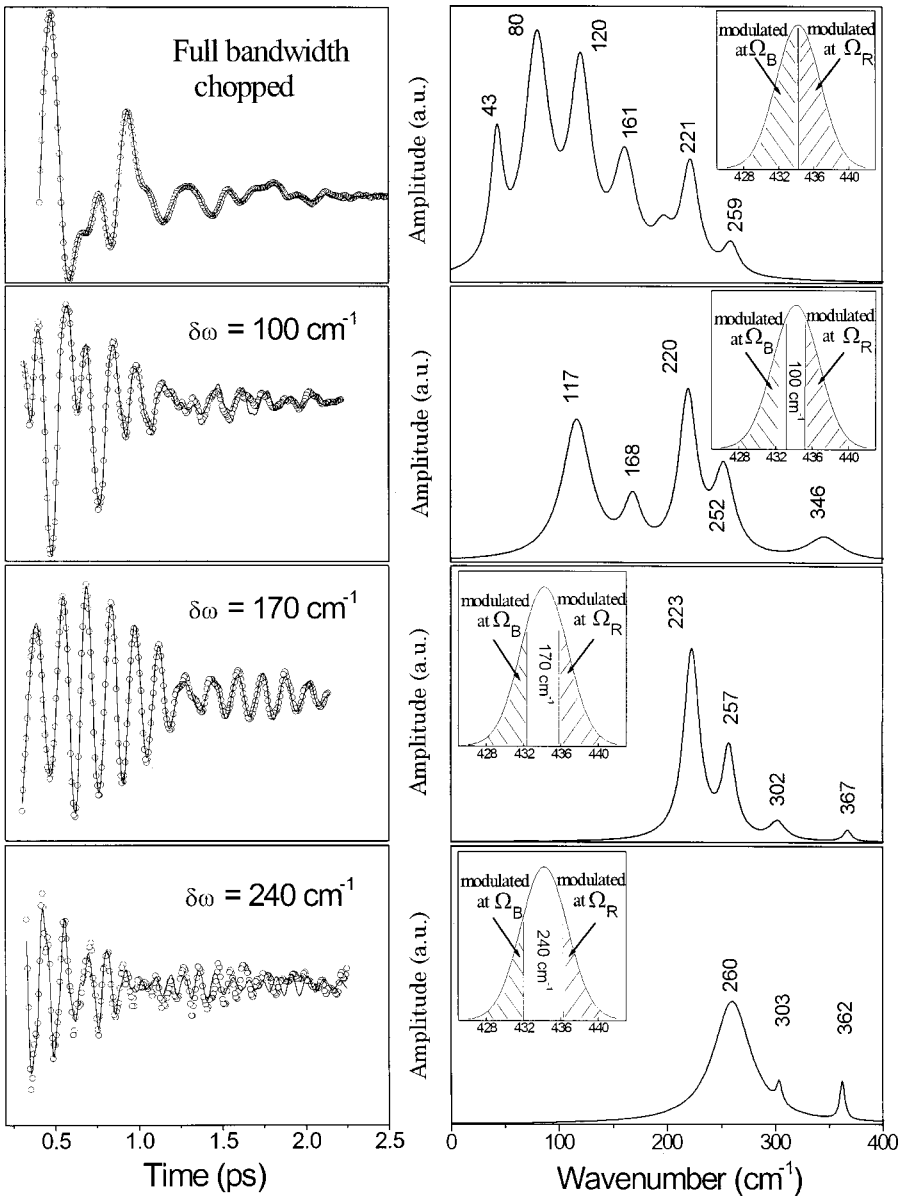

FIG. 9. Sequence of experiments using frequency selective pump modulation on MbNO. The left panels show the generated FCS signals (in circles) and their LPSVD fit (solid line), whereas the right panels show the corresponding power spectra. The insets depict the spectral regions of the pump pulse modulated by the two fork choppers.

that the feature near 20 cm^{-1} in the neutron scattering experiments involves a more global protein motion. Since the FCS experiments on the FePPIX model compound also demonstrate that a local heme mode exists near 20 cm^{-1}, we suggest that the active site (heme) and the protein are potentially coupled energetically through the near degeneracy of these modes. Recent protein photoacoustic experiments demonstrate that the dominant displacement or strain along the reaction coordinate develops on a 2 ps time scale.[13] Both the oscillatory period (1.6 ps) and damping constant (1–1.5 ps) of the observed ~20 cm^{-1} mode are in excellent agreement with such time scales. The observed[46–51] time scales of motion over all available length scales (from changes in the vicinity of the heme site to the global, protein-solvent motions) are approximately the same, suggesting the presence of highly correlated dynamics in myoglobin (see also Ref. 41).

It is also possible that the rapid transfer of the heme localized excitation energy (after the pump pulse interaction) to the protein material explains the much shorter lifetime of the ~20 cm^{-1} mode in the ligated samples (MbNO, HbNO). Upon dissociation of the diatomic ligand, the initial heme localized forces rapidly redistribute the vibrational energy by acting upon the surrounding protein. The nonconservative work resulting in the MbNo→Mb protein structural rearrangements, done by the reaction induced forces, would be expected to increase the damping constant of the ~20 cm^{-1} mode in the ligated samples. Structural relaxation of the protein can also be inferred from the changes of the Fe–His frequency following the photodissociation reaction.[12,52] Since the pump pulse interaction with the photostable samples (i.e., equilibrium deoxy Mb) does not lead to large nonequilibrium displacements or major protein structural rearrangements, the energy of the ~20 cm^{-1} oscillations in these samples is dissipated at a slower rate, yielding the longer lifetimes. Finally, it should be noted that a resonant coupling mechanism between the heme and the protein material (involving the ~20 cm^{-1} mode) is conceivably in-

volved in the dynamics of hemoglobin cooperativity, which links the oxygen affinity of one heme active site to the bound or unbound state of other active sites within the protein.

In addition to the 20 cm^{-1} mode, one also observes in Fig. 8 the existence of a strong ~ 40 $cm{-}^{1}$ mode. The presence of this mode in deoxy myoglobin (and in most of the heme proteins studied to date) implies that it is unlikely that this mode arises from coherent population transfer between the ligand bound and unbound states as recently suggested for cytochrome oxidase.[36] This is because the deoxy samples are not involved in ligand exchange reactions. It is possible[53] that the appearance of the ~ 40 cm^{-1} mode in deoxy Mb is a coincidence and arises from a completely different mechanism than the ~ 40 cm^{-1} mode associated with ligand dissociation in Mb and cytochrome oxidase. However, the fact that the ~ 40 cm^{-1} mode is observed in the wavelength selective probe beam modulation experiments, which discriminates against population induced signals, speaks strongly against the proposed coherent population transfer model[36] as a source of the ~ 40 cm^{-1} oscillation, at least in MbNO.

The observation of oscillatory signals in the pump beam wavelength selective modulation experiments performed on NO bound myoglobin yields further information regarding the photodissociation mechanism. Since the technique is sensitive only to processes triggered by the intervention of two pump fields of different color, the signals arising from transient population dynamics are almost completely eliminated. In the nonadiabatic dissociation model,[39] the vibrational coherence is triggered by photon absorption (two fields of the same color) and subsequent rapid electronic surface crossing associated with the ligand dissociation induced iron spin-state change (from $S=0$ to $S=2$). In this model, the coherent signal is expected to diminish when using the wavelength selective pump modulation, since the population terms are discriminated against. This expectation is contradicted by the experimental results presented in Fig. 9, which demonstrate that the vibrational coherence observed in the reactive samples is generated directly from the optical frequencies available in the femtosecond pump pulse. This is a remarkable observation, particularly for the 220 cm^{-1} Fe–His mode, since it is not observed in the resonance Raman spectrum of the reactant (MbNO) and is not expected to be coupled to the resonant optical transition. The dissociative surface accessed by the pump pulse fields evidently supports the 220 cm^{-1} oscillation, providing strong evidence that ligand dissociation proceeds directly upon photoexcitation.

A related observation is the previously reported phase measurement of the 220 cm^{-1} Fe–His stretching mode in MbNO.[11] Its phase is measured to be either 0 or π as the carrier frequency of the laser pulse is tuned across the product state (deoxy Mb) absorption band. These values of the absolute phase imply that the coherence of the Fe–His mode is generated nearly instantaneously, without a significant delay associated with the reaction time, which would shift the phase of the 220 cm^{-1} mode away from 0 or π. For example, if we assume that the reaction time is ~ 30 fs (half the period of the Fe–NO mode), a comparison to the period of the Fe-His mode (150 fs) yields a nonzero initial phase ($\Phi \cong 72°$). Nevertheless, since the Fe–His mode is Raman inactive in the NO bound sample, the observed signal must be associated with the deoxy myoglobin product state.

One possible explanation for these observations is that an adiabatic (strong coupling) model provides a better description of the dissociation process. In such a model the iron spin states of the reactant (MbNO) and the product (deoxy Mb) are not pure ($S=0$ and $S=2$, respectively), but rather have a certain degree of admixture associated with them, allowing for direct electric dipole coupling between the reactant and product states. In the nonadiabatic model, it is generally assumed[39] that the electric dipole coupling between the reactant (MbNO, $S=0$) and product (Mb, $S=2$) states is forbidden based on spin selection rules. This means that only a chemical reaction (i.e., rapid ligand dissociation after the fields have ceased to evolve) can access the final product state and lead to coherence in the coupled degrees of freedom.

On the other hand, there are experimental results suggesting that iron spin admixtures do exist in deoxy Mb and deoxy Hb. Measurements of the magnetic moments for phosphate-free and phosphate-bound deoxy Hb generated different results,[54] and it has been suggested that molecular vibrations can affect the spin state of the iron atom.[55] The calculated[56–58] energy gap between the ground spin state and other higher lying electronic spin states is at most a few hundred cm^{-1}, which is well within the range of thermally excited nuclear vibrations. The existence of direct electric dipole coupling between the reactant and product states allows the pump pulse to directly generate product state coherences, as the photodissociation reaction takes place. The presence of such coupling is consistent with the observation that multiple optical frequencies within the pump pulse are needed for the generation of coherences in MbNO. It is also consistent with the fact that the phase of the (Raman inactive) Fe–His mode is found to be 0 or π in the MbNO sample. Such observations provide strong support for an adiabatic strong coupling model in MbNO.

The presence of spin state admixtures could impact the characteristics of NO recombination, following the photodissociation reaction. The large amplitude ($I_g \sim 95\%$) and fast rate ($\tau_g \sim 10–100$ ps)[59,60] of the NO geminate recombination to deoxy Mb differ considerably from the corresponding characteristics of CO ($I_g \sim 5\%$ with $\tau_g \sim 100$ ns)[61] and O_2 ($I_g \sim 58\%$ with $\tau_g \sim 25$ ns).[62] The geminate rate is likely to be affected by the iron spin changes associated with the ligand recombination. Thus, a strong iron spin admixture in MbNO could help to explain the increased NO geminate rates and the dramatic differences between the recombination characteristics of NO, CO, and O_2.

ACKNOWLEDGMENTS

This work was supported by NSF MCB9904516 and NIH DK35090.

APPENDIX: ANALYSIS OF PUMP WAVELENGTH SELECTIVE MODULATION EXPERIMENTS

We consider a linearly coupled two electronic level system, initially in the ground electronic state, with a vibrational

density matrix $\hat{\rho}_T$. The pulse-induced nuclear density matrix in the excited state is given by (to second order in the laser fields)

$$\hat{\rho}_e=\frac{\mu^2}{\hbar^2}\int_{-\infty}^{\infty}dt'\int_{-\infty}^{\infty}dt''E(t')E(t'')\times\{e^{i\Omega_{00}(t'-t'')}e^{i\hat{H}_e t'/\hbar}e^{-i\hat{H}_g t'/\hbar}\hat{\rho}_T e^{i\hat{H}_g t''/\hbar}e^{-i\hat{H}_e t''/\hbar}\}, \tag{A1}$$

where $\hat{H}_g$ and $\hat{H}_e$ are, respectively, the adiabatic Born–Oppenheimer Hamiltonians for the ground and excited electronic states, μ is the electronic dipole moment, and Ω_{00} is the 0–0 transition energy. In order to calculate the density matrix relevant for wavelength selective modulation of the pump pulse, we split the electric field into components on the red and blue sides of the carrier frequency

$$E(t)=\cos(\Omega_R t)E_R(t)+\cos(\Omega_B t)E_B(t), \tag{A2}$$

where

$$E_R(t)=\frac{1}{\pi}\int_0^{\omega_c-\delta\omega/2}d\omega G(\omega-\omega_c)\cos(\omega t), \tag{A3a}$$

$$E_B(t)=\frac{1}{\pi}\int_{\omega_c+\delta\omega/2}^{\infty}d\omega G(\omega-\omega_c)\cos(\omega t). \tag{A3b}$$

In the above expressions, $G(\omega-\omega_c)$ is the Fourier transform of the pump pulse spectral envelope, which is taken as a Gaussian centered at the carrier frequency ω_c. $\delta\omega$ is the spacing between the blades of the choppers, which independently modulate the red and blue spectral regions of the pulse at frequencies Ω_R and Ω_B, respectively (Ω_R and Ω_B are much smaller than the optical frequency).

When Eqs. (A2)–(A3b) are used in Eq. (A1), four terms result, proportional to the products $E_R E_B$, $E_B E_R$, $E_R E_R$, and $E_B E_B$. Of these four terms, wavelength selective modulation selects only the first two terms, which are modulated at the sum frequency $\Omega_R+\Omega_B$. Considering only these terms, we evaluate the elements of the excited state density matrix $(\hat{\rho}_e^{RB})_{vv'}=\langle v_e|\hat{\rho}_e^{RB}|v_e'\rangle$, where $|v_e\rangle$ is the vth vibrational eigenstate of the excited electronic state. Assuming that the system is initially in the ground vibrational level of the electronic state $|g\rangle$, i.e., $\hat{\rho}_T=|0_g\rangle\langle 0_g|$, we get

$$(\hat{\rho}_e^{RB})_{vv'}=\frac{\mu^2F_{v,v'}}{\pi^2\hbar^2}\int_0^{\omega_c-\delta\omega/2}d\omega\int_{\omega_c+\delta\omega/2}^{\infty}d\omega' G(\omega-\omega_c)\times G(\omega'-\omega_c)\int_{-\infty}^{\infty}dt'\int_{-\infty}^{\infty}dt''\,e^{i(\Omega_{00}+v'\omega_0)s}\times e^{i(v-v')\omega_0 t'}[\cos(\omega t')\cos(\omega' t'')+\cos(\omega t'')\cos(\omega' t')], \tag{A4}$$

where $F_{v,v'}=\langle v_e|0_g\rangle\langle 0_g|v_e'\rangle$ and $s=t'-t''$. Note that $F_{v,v}$ is simply the Franck–Condon overlap factor between the ground and excited vibrational states. Performing the integrals above and ignoring small contributions from nonresonant terms (rotating wave approximation), we get

$$(\hat{\rho}_e^{RB})_{vv'}=\frac{\mu^2F_{v,v'}}{2\pi\hbar^2}\int_0^{\omega_c-\delta\omega/2}d\omega\int_{\omega_c+\delta\omega/2}^{\infty}d\omega' G(\omega-\omega_c)\times G(\omega'-\omega_c)[\Phi_v(\omega)\delta(\omega-\omega'-k\omega_0)+\Phi_{v'}(\omega)\delta(\omega-\omega'+k\omega_0)], \tag{A5}$$

where $k=v-v'$ and

$$\Phi_v(\omega)=\int_{-\infty}^{\infty}ds\,e^{i(\omega-\Omega_{00}-v\omega_0)s}=2\pi\delta(\omega-\Omega_{00}-v\omega_0) \tag{A6}$$

is defined as a spectral line shape function. To obtain Eq. (A5), we have used the relation $\Phi_{v'}(\omega-k\omega_0)=\Phi_v(\omega)$. Since $\omega<\omega'$ (which follows from the integration limits, with $\delta\omega>0$), the first term in the square brackets in Eq. (A5) contributes for $v<v'$ and the second term contributes when $v>v'$. It is also verified that $(\hat{\rho}_e^{RB})_{vv'}=(\hat{\rho}_e^{RB})^*_{v'v}$.

It is clear from Eq. (A5) that $(\hat{\rho}_e^{RB})_{vv'}=0$ if $\delta\omega>|(v-v')|\omega_0$, since the two frequency integrals in Eq. (A5) are nonoverlapping. This accounts for the sharp frequency selection of vibrational modes as $\delta\omega$ is varied. In particular, we see that the zero frequency diagonal elements, $(\hat{\rho}_e^{RB})_{vv}=0$, provided $\delta\omega>0$. This in turn accounts for the absence of population terms in the signal channel detected at $\Omega_R+\Omega_B$.

The above expressions assumed that there were no electronic dephasing mechanisms. One way to introduce electronic dephasing is to make Ω_{00} complex. This would amount to introducing a factor $\exp(-\Gamma_c|s|)$ in Eq. (A1). Γ_c could be identified with dephasing of the electronic coherence between the ground and excited electronic states.[33,62] Since Ω_{00} appears in the above expressions only through $\Phi_v(\omega)$ in Eq. (A6), it is clear that the sharp frequency selection and the suppression of the population terms would still be feasible using a wavelength selective modulation followed by detection at $\Omega_R+\Omega_B$.

In contrast to electronic dephasing processes, vibrational dephasing can affect the resolution of the wavelength selective modulation. To see this, we introduce vibrational damping through the factor $\exp(-\gamma_v|t|/2)$ on the bra and ket side interactions in Eq. (A1). This corresponds to the transformation $\hat{H}_e\rightarrow\hat{H}_e\pm i\gamma_v/2$. In this case, we immediately find

$$(\hat{\rho}_e^{RB})_{vv'}=\frac{\mu^2F_{v,v'}}{4\pi^2\hbar^2}\int_0^{\omega_c-\delta\omega/2}d\omega\int_{\omega_c+\delta\omega/2}^{\infty}d\omega' G(\omega-\omega_c)\times G(\omega'-\omega_c)[\Phi_v(\omega)\Phi_{v'}(\omega')+\Phi_{v'}(\omega)\Phi_v(\omega')], \tag{A7}$$

where the line shape function is now a Lorentzian rather than a delta function

$$\Phi_v(\omega)=\int_{-\infty}^{\infty}ds\,e^{-\gamma_v|s|/2}e^{i(\omega-\Omega_{00}-v\omega_0)s}. \tag{A8}$$

It is clear from Eq. (A7) that even when the condition $\delta\omega>|(v-v')|\omega_0$ is satisfied, $(\hat{\rho}_e^{RB})_{vv'}$ does not necessarily vanish. This is due to the spectrally broad line shape functions that take the place of the delta functions in Eq. (A5). It

is easily verified that when $\gamma_v = 0$, the line shape reduces to a delta function as in Eq. (A6), and if we use the identity $\delta(a-x)\,\delta(b-x) = \delta(a-x)\,\delta(a-b)$, $(\hat{\rho}_e^{RB})_{vv'}$ reduces to the result in Eq. (A5).

[1] M. Chachisvilis, H. Fidder, and V. Sundstrom, Chem. Phys. Lett. **234**, 141 (1995).
[2] J. C. Polanyi and A. H. Zewail, Acc. Chem. Res. **28**, 119 (1995).
[3] N. Pugliano, A. Z. Szarka, and R. M. Hochstrasser, J. Chem. Phys. **104**, 5062 (1996).
[4] N. F. Scherer, D. M. Jonas, and G. R. Fleming, J. Chem. Phys. **99**, 153 (1993).
[5] W. H. Vos, F. Rappaport, J. C. Lambry, J. Breton, and J. L. Martin, Nature (London) **363**, 320 (1993).
[6] L. D. Book, D. C. Arnett, H. B. Hu, and N. F. Scherer, J. Phys. Chem. A **102**, 4350 (1998).
[7] T. S. Yang, M. S. Chang, R. Chang, M. Hayashi, S. H. Lin, P. Vohringer, W. Dietz, and N. F. Scherer, J. Chem. Phys. **110**, 12070 (1999).
[8] Q. Wang, R. W. Schoenlein, L. A. Peteanu, R. A. Mathies, and C. V. Shank, Science **266**, 422 (1994).
[9] L. Y. Zhu, J. T. Sage, and P. M. Champion, Science **266**, 629 (1994).
[10] L. D. Ziegler, R. Fan, A. E. Desrosiers, and N. P. Scherer, J. Chem. Phys. **100**, 1823 (1994).
[11] F. Rosca, A. T. N. Kumar, X. Ye, T. Sjodin, A. A. Demidov, and P. M. Champion, J. Phys. Chem. **104**, 4280 (2000).
[12] P. M. Champion, F. Rosca, W. Wang, A. T. N. Kumar, J. Christian, and A. Demidov, in *Laser Techniques for Condensed-Phase and Biological Systems*, Proc. SPIE **3273**, 80 (1998).
[13] J. Deak, H. L. Chin, C. M. Lewis, and R. J. D. Miller, J. Phys. Chem. B **102**, 6621 (1998).
[14] R. J. D. Miller, Acc. Chem. Res. **27**, 145 (1994).
[15] L. Richard, L. Genberg, J. Deak, H. L. Chiu, and R. J. D. Miller, Biochemistry **31**, 10703 (1992).
[16] L. Zhu, P. Li, J. T. Sage, and P. M. Champion, J. Lumin. **60-1**, 503 (1994).
[17] H. Barkhuijsen, R. De Beer, W. M. M. J. Bovee, and D. Van Ormondt, J. Magn. Reson. **61**, 465 (1985).
[18] F. Wise, M. Rosker, G. Millhauser, and C. L. Tang, IEEE J. Quant. Electron. **QE-23**, 1116 (1987).
[19] S. Mazumdar, J. Chem. Soc. Dalton Trans. **1991**, 2091.
[20] D. Barrick and F. W. Dahlquist, Proteins: Struct., Funct., Genet. **39**, 278 (2000).
[21] D. Barrick, Proteins: Struct., Funct., Genet. **39**, 291 (2000).
[22] H. Kawashima, M. M. Wefers, and K. A. Nelson, Annu. Rev. Phys. Chem. **46**, 627 (1995).
[23] E. B. Treacy, IEEE J. Quantum Electron. **5**, 454 (1969).
[24] P. M. Kozlowski, T. G. Spiro, A. Berces, and M. Z. Zgierski, J. Phys. Chem. B **102**, 2603 (1998).
[25] T. G. Spiro, P. M. Kozlowski, and M. Z. Zgierski, J. Raman Spectrosc. **29**, 869 (1998).
[26] S. Constantine, Y. Zhou, J. Morais, and L. D. Ziegler, J. Phys. Chem. A **101**, 5456 (1997).
[27] J. Zhou, S. Constantine, S. Harrel, and L. D. Ziegler, J. Chem. Phys. **110**, 5893 (1999).
[28] A. T. N. Kumar, F. Rosca, A. Widom, and P. M. Champion, J. Chem. Phys. **114**, 701 (2001).
[29] M. H. Cho, G. R. Fleming, and S. Mukamel, J. Chem. Phys. **98**, 5314 (1993).
[30] Y. J. Yan and S. Mukamel, Phys. Rev. A **41**, 6485 (1990).
[31] B. Fain and S. H. Lin, Chem. Phys. **161**, 515 (1992).
[32] B. Fain and S. H. Lin, Chem. Phys. Lett. **207**, 287 (1993).
[33] A. M. Walsh and R. F. Loring, Chem. Phys. Lett. **160**, 299 (1989).
[34] S. Mukamel, *Principles of Nonlinear Optical Spectroscopy* (Oxford University Press, New York, 1995).
[35] A. T. N. Kumar, F. Rosca, A. Widom, and P. M. Champion, J. Chem. Phys. **114**, 6795 (2001).
[36] U. Liebl, G. Lipowski, M. Negrerie, J. C. Lambry, J. L. Martin, and M. H. Vos, Nature (London) **401**, 181 (1999).
[37] Note that ferrous FePPIX under the condition of 433 nm excitation does not display a mode near 40 cm^{-1} as might be expected. However, when the excitation is tuned to 440 nm, this mode is clearly resolved, but with a shorter lifetime than in Mb. On the other hand, ferric FePPIX displays a strong 40 cm^{-1} mode under a broad range of excitation conditions. A detailed presentation and analysis of the signal at 40 cm^{-1} will be presented elsewhere.
[38] In horse heart cytochrome c, the PP IX structure is perturbed by thiolether bridges to the heme (at R_2 and R_4) from two cysteine side chains (Cys14 and Cys17). The iron is also coordinated to a histidine (His 18) and methionine (Met 80). Octapeptide (microperoxidase-8) is produced from the digestion of horse heart cytochrome c to a peptide chain of residues 14–21. The heme is still bound to the peptide by 2 thiolether bridges and a histidine. Iron octaethylporphyrin is a symmetric porphyrin where 8 ethyl groups are bound to the porphyrin macrocycle.
[39] L. Y. Zhu, A. Widom, and P. M. Champion, J. Chem. Phys. **107**, 2859 (1997).
[40] L. Findsen, D. Bocian, and R. Birge, J. Chem. Phys. **88**, 7588 (1988).
[41] J. T. Sage, S. M. Durbin, W. Sturhahn, D. C. Wharton, P. M. Champion, P. Hession, J. Sutter, and E. E. Alp, Phys. Rev. Lett. **86**, 4966 (2001).
[42] H. Leyser, W. Doster, and M. Diehl, Phys. Rev. Lett. **82**, 2987 (1999); W. Doster, S. Cusack, and W. Petry, Nature (London) **337**, 754 (1989).
[43] J. C. Smith, Q. Rev. Biophys. **24**, 227 (1991).
[44] J. S. Ahn, Y. Kanematsu, M. Enomoto, and T. Kushida, Chem. Phys. Lett. **215**, 336 (1993).
[45] Y. Seno and N. Go, J. Mol. Biol. **216**, 95 (1990).
[46] J. M. Friedman, T. W. Scott, G. J. Fisanick, S. R. Simon, E. W. Findsen, M. R. Ondrias, and V. W. Macdonald, Science **229**, 187 (1985).
[47] J. W. Petrich, J. L. Martin, D. Houde, C. Poyart, and A. Orszag, Biochemistry **26**, 7914 (1987).
[48] R. Lingle, X. B. Xu, H. P. Zhu, S. C. Yu, and J. B. Hopkins, J. Phys. Chem. **95**, 9320 (1991).
[49] P. Li, J. T. Sage, and P. M. Champion, J. Chem. Phys. **97**, 3214 (1992).
[50] M. Lim, T. A. Jackson, and P. A. Anfinrud, Proc. SPIE **1921**, 221 (1992).
[51] M. Lim, T. A. Jackson, and P. A. Anfinrud, Proc. Natl. Acad. Sci. U.S.A. **90**, 8302 (1993).
[52] J. T. Sage, K. T. Schomacker, and P. M. Champion, J. Phys. Chem. **99**, 3394 (1995).
[53] J. L. Martin, private communication (2000).
[54] Y. Alpert and R. Banerjee, Biochim. Biophys. Acta **405**, 144 (1975).
[55] M. Bacci, J. Chem. Phys. **68**, 4907 (1978).
[56] B. H. Huynh, G. C. Papaefthymoiu, C. S. Yen, J. L. Groves, and C. S. Wu, J. Chem. Phys. **61**, 3750 (1974).
[57] A. Trautwein, R. Zimmermann, and F. E. Harris, Theor. Chim. Acta **37**, 89 (1975).
[58] H. Eicher, D. Bade, and F. Parak, J. Chem. Phys. **64**, 1446 (1976).
[59] Y. Kholodenko, E. A. Gooding, Y. Dou, M. Ikeda-Saito, and R. M. Hochstrasser, Biochemistry **38**, 5918 (1999).
[60] D. Ionascu and F. Rosca (unpublished).
[61] W. D. Tian, J. T. Sage, and P. M. Champion, J. Mol. Biol. **233**, 155 (1993).
[62] K. N. Walda, X. Y. Liu, V. S. Sharma, and D. Magde, Biochemistry **33**, 2198 (1994).